

MODELLING HIGH SCHMIDT NUMBER TURBULENT SCALAR TRANSPORT ACROSS AIR-WATER INTERFACES

K. Suga and M. Kubo

Department of Mechanical Engineering,
Osaka Prefecture University
1-1 Gakuen-cho, Naka-ku, Sakai, 599-8531, Japan
suga@me.osakafu-u.ac.jp, kubo@htlab.me.osakafu-u.ac.jp

ABSTRACT

An extended version of the analytical wall-function (AWF) is presented for solving mass transfer fields across air-water interfaces. By considering exact near-surface limiting profiles of turbulence quantities such as the eddy viscosity and the turbulent scalar flux, the prescribed turbulent diffusivity profile, which is a core assumption of the AWF, is modelled to have the correct limiting behaviour. The resultant AWF performs well to predict turbulent concentration fields under air-water interfaces at the Schmidt numbers of $1 \leq Sc \leq 1000$.

INTRODUCTION

Although wall bounded flows and free surface flows share some similar characteristics, they have many definitely different points in mass transfer characteristics. Since working liquid in industrial machinery is often bounded by free surfaces, it is essential to understand the flow and scalar characteristics near free-surfaces for designing such fluid machines. Moreover, liquid-gas free surfaces are common in environmental issues and turbulent mass transfer across liquid interfaces is very important.

Liquid-side free surface turbulence thus has been experimentally investigated by several researchers such as Rashidi & Banerjee (1988) and Komori *et al.* (1989). Measurements of the turbulent mass transfer mechanism near free-surfaces have been less extensive since there is difficulty in analysing the phenomena due to that the scalar (concentration of a solute) boundary-layer is very much thinner than that of the flow boundary-layer. The Schmidt number Sc is, indeed, in the order of $O(10^3)$ in the liquid side. In this condition, the scalar boundary layer thickness becomes 10 % of the flow boundary layer thickness. Although thanks to the recent development of laser induced fluorescence (LIF) techniques, such difficulty is now being cleared (Herlina & Jirka, 2008; Walker Peirson, 2008), space resolved accurate experiments of free surface mass transfer are still rather difficult compared with those of flow fields.

Numerical approaches are thus promising. Detailed flow structures have been revealed by several direct numerical simulation (DNS) studies (e.g. Komori *et al.*, 1993; Lombardi *et al.*, 1996). Calmet & Magnaudet (1998) and Hasegawa & Kasagi (2007) performed numerical simulations to investigate the detailed mass transfer mechanisms by respectively large eddy simulation (LES) and DNS techniques.

Although lots of knowledge on the flow and mass transfer mechanisms has been accumulated as above, not so many studies have discussed on engineeringly practical schemes to estimate those phenomena. Suga & Abe (2000) discussed a low Reynolds number (LRN) nonlinear three-equation eddy viscosity model to predict free surface scalar transfer. LRN

models, which require high grid resolutions for capturing fine-scale flow and scalar transfer near-surfaces, however, are not very practical for an environmental issue, unfortunately. For example, in order to discuss the amount of the absorption of atmospheric carbon dioxide (CO_2) at the sea surface, one should obtain turbulent mass transfer across the large air-sea interface.

Therefore, in order to provide a truly practical strategy, the present study develops a scheme which treats high Schmidt number free surface turbulent mass transport. The basic idea employed is the analytical wall-function (AWF) approach originally proposed by Craft *et al.* (2002) for wall turbulence. With this approach, one only needs rather coarse wall-function grids instead of fine grids resolving the thin boundary-layers. In fact, Suga (2007) successfully obtained high Prandtl number wall heat transfer by extending the AWF approach with consideration of the near-wall limiting behaviour of the eddy viscosity. The present modelling scheme thus follows this modelling strategy.

NOMENCLATURE

A_U, A_C : integration constants
 c, \bar{c} : concentration and mean concentration of a solute
 c_ℓ, c_μ : model constants
 C_C : sum of the convection and the diffusion terms of the scalar equation
 C_U : sum of the convection and the diffusion terms of the momentum equation
 k, k_P : turbulence energy, k at node P
 P : pressure or cell centre of the wall adjacent cell
 P_k : production term of k equation
 Sc : Schmidt number
 Sc_t, Sc_t^∞ : turbulent Schmidt numbers
 q_s : surface concentration flux
 Re_τ : friction Reynolds number: $u_\tau \delta / \nu$
 $\overline{u_i u_j}$: Reynolds stress
 u_τ, U^+ : friction velocity, U/u_τ
 U, V : mean velocity components
 $-\rho \bar{v} \bar{c}$: turbulent concentration flux
 y_v, y_c : viscous sub-layer thicknesses
 y^* : normalized distance: $y \sqrt{k_P} / \nu$
 α, α_c : $c_\mu c_\ell, \kappa / y_c^*$
 α_{ct}, α_{cd} : $\kappa Sc / Sc_t, \alpha_{ct} / y_c^*$
 β : model coefficient
 ϵ : turbulent diffusivity
 δ : boundary layer thickness
 ϵ : dissipation rate of k
 κ^* : coefficient of turbulent length scale: $\alpha \beta$
 μ, μ_t : viscosity, turbulent viscosity
 ν, ν_t : kinematic viscosity, kinematic turbulent viscosity
 ρ : fluid density
 τ_s : surface shear stress

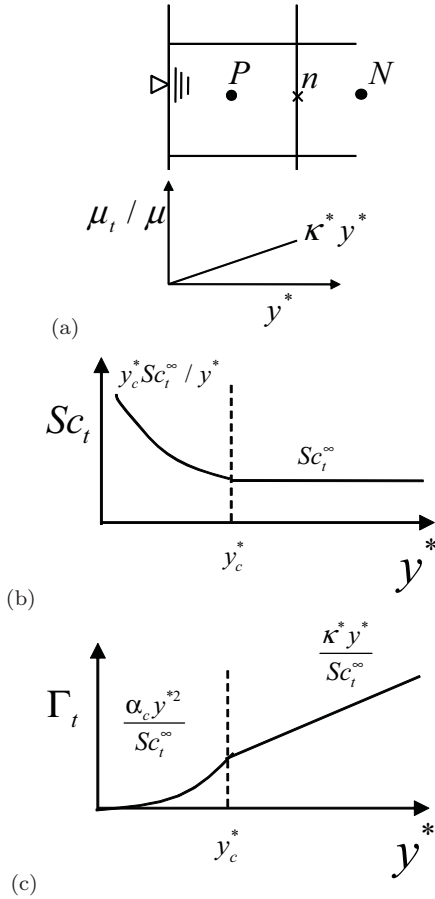


Figure 1: Near-surface distribution:(a)near-surface cell arrangement and the eddy viscosity distribution, (b)turbulent Schmidt number distribution, (c)turbulent diffusivity distribution.

AWF MODELLING FOR HIGH SCHMIDT NUMBER FLOWS

Flow field modelling

In the AWF for wall turbulence, the wall shear stress and scalar flux are obtained through the analytical solution of simplified near-wall versions of the transport equations for the wall-parallel momentum and scalar. In case of forced convection regimes, the main assumption required for the analytical integration of the transport equations is a prescribed variation of the turbulent viscosity μ_t . The distribution of μ_t over the wall adjacent cell P is modelled as in a one-equation turbulence model:

$$\mu_t = \rho c_\mu k^{1/2} \ell = \rho c_\mu k^{1/2} c_\ell y \simeq \alpha \mu y^*, \quad (1)$$

where ℓ is the turbulent length scale, $\alpha = c_\ell c_\mu$ and $y^* \equiv y k_P^{1/2} / \nu$. (The coefficients $c_\ell = 2.55$, $c_\mu = 0.09$ are used.)

In the wall turbulence, it is well known that the theoretical limiting variations of the velocity components and their fluctuations are

$$\begin{aligned} u &= b_u y + c_u y^2 + \dots, \\ v &= c_v y^2 + \dots, \\ u' &= b'_u y + c'_u y^2 + \dots, \\ v' &= c'_v y^2 + \dots. \end{aligned} \quad (2)$$

Since the eddy viscosity relates the Reynolds stress with the mean velocity gradient as $-\rho \overline{uv} = \mu_t \partial U / \partial y$, the above

relations lead to

$$-\rho \{ \overline{b'_u c'_v} y^3 + \dots \} = \mu_t (\overline{b_u} + \dots), \quad (3)$$

and it is obvious that $\mu_t \propto O(y^3)$ in the viscous sublayer. Since Eq.(1) does not satisfy this limiting condition, near-wall damping is normally applied. However, in order to consider the viscous sub-layer effects without a damping function, Craft *et al.*(2002) modelled the profile of μ_t as

$$\mu_t = \alpha \mu \max \{ 0, (y^* - y_v^*) \}, \quad (4)$$

in which μ_t is still linear in y^* and grows from the edge of the viscous sub-layer y_v . Although this form still does not satisfy the limiting condition, it was confirmed that the effects of such un-satisfaction were marginal for low fields (Suga, 2007).

In contrast to the wall turbulence, the theoretical limiting variations of the velocity components and their fluctuations near a gas-liquid interface are

$$\begin{aligned} u &= a_u + b_u y + c_u y^2 + \dots, \\ v &= a_v + b_v y + c_v y^2 + \dots, \\ u' &= a'_u + b'_u y + c'_u y^2 + \dots, \\ v' &= a'_v + b'_v y + c'_v y^2 + \dots. \end{aligned} \quad (5)$$

Thus, the above relations lead to

$$-\rho \{ \overline{a'_u a'_v} + (\overline{a'_u b'_v} + \overline{a'_v b'_u}) y + \dots \} = \mu_t (b_u + 2 \overline{c_u} y + \dots), \quad (6)$$

and it is obvious that $\mu_t \propto O(y^0)$. Thus, the near-interface variation of μ_t can be modelled as:

$$\mu_t = \kappa^* \mu \max \{ 0, (y^* - y_v^*) \} \quad (7)$$

where y_v^* can be negative to make the interface flow “rough turbulence”. (In such a case, y_v is no longer the viscous sub-layer thickness.) This form is the same as in the rough-wall AWF of Suga *et al.*(2006). The model coefficient κ^* is now rewritten as $\kappa^* = \alpha \beta$ with β , a factor of modifying the turbulence distribution for the near free-surface regions.

In the case of non-surface-disturbance where $a'_v = 0$, Eq.(7) needs to be $\mu_t = \kappa^* \mu y^*$ as in Fig.1(a) since Eq.(6) leads to $\mu_t \propto O(y)$. Then, the near-wall simplified momentum equation:

$$\frac{\partial}{\partial y^*} \left[(\mu + \mu_t) \frac{\partial U}{\partial y^*} \right] = \underbrace{\frac{\nu^2}{k_P} \left[\frac{\partial}{\partial x} (\rho U U) + \frac{\partial P}{\partial x} \right]}_{C_U}, \quad (8)$$

can be integrated over the cell P analytically as

$$\frac{dU}{dy^*} = \frac{C_U y^* + A_U}{\mu \{ 1 + \kappa^* y^* \}}, \quad (9)$$

$$U = \frac{C_U}{\kappa^* \mu} y^* + \left\{ \frac{A_U}{\kappa^* \mu} - \frac{C_U}{\kappa^{*2} \mu} \right\} \ln [1 + \kappa^* y^*] + B_U. \quad (10)$$

The integration constants A_U, B_U are determined by applying boundary conditions at the free surface s and the cell face n :

$$A_U = \frac{\kappa^* \mu (U_n - U_s) - C_U y_n^*}{\ln(1 + \kappa^* y_n^*)} + \frac{C_U}{\kappa^*}, \quad (11)$$

$$B_U = U_s. \quad (12)$$

The values at n are determined by interpolation between the calculated node values at P and N . The surface shear stress is then obtained as

$$\tau_s = \mu \left. \frac{dU}{dy} \right|_s = \mu \frac{k_P^{1/2}}{\nu} \left. \frac{dU}{dy^*} \right|_s = \frac{k_P^{1/2} A_U}{\nu}. \quad (13)$$

Table 1: Proposed model coefficients for non-disturbance free-surface.

κ^*	α	α_c	β	c_μ	c_ℓ	y_c^*	Sc_t^∞
$\alpha\beta$	$c_\mu c_\ell$	κ^*/y_c^*	0.55	0.09	2.55	11.7	0.9

The local generation rate of k , $P_k (= \nu_t (\frac{dU}{dy})^2)$, is written as

$$P_k = \frac{\kappa^* k_P y^*}{\nu} \left(\frac{C_U y^* + A_U}{\mu \{1 + \kappa^* y^*\}} \right)^2, \quad (14)$$

which can then be integrated over the wall-adjacent cell to produce an average value $\overline{P_k}$ for solving the k equation as

$$\begin{aligned} \overline{P_k} &= \frac{\kappa^* \rho k_P}{\mu^3 y_n^*} \int_0^n y^* \left(\frac{C_U y^* + A_U}{1 + \kappa^* y^*} \right)^2 dy^* \\ &= \frac{\kappa^* \rho k_P}{\mu^3 y_n^*} \left[\frac{C_U^2}{2\kappa^{*2}} y^{*2} + \frac{C_U(2A_U - 2C_U/\kappa^*)}{\kappa^{*2}} y^* \right. \\ &\quad \left. + \frac{\{A_U - C_U/\kappa^*\}^2}{\kappa^{*2}(1 + \kappa^* y^*)} + \{A_U - C_U/\kappa^*\} \right. \\ &\quad \left. \times \frac{\{A_U - 3C_U/\kappa^*\}}{\kappa^{*2}} \ln(1 + \kappa^* y^*) \right]_0^n \quad (15) \end{aligned}$$

For wall turbulence, the following model of the dissipation rate of k :

$$\varepsilon = \begin{cases} 2\nu k_P / y_\varepsilon^2, & \text{if } y < y_\varepsilon \\ k_P^{1.5} / (c_\ell y), & \text{if } y \geq y_\varepsilon \end{cases} \quad (16)$$

was employed in the AWF by Craft *et al.*(2002) with the characteristic dissipation scale y_ε . However, at the free surface, the value of ε is

$$\varepsilon_s = \nu(\overline{b_u'^2} + \overline{b_v'^2} + \overline{b_w'^2}), \quad (17)$$

which is slightly different from the wall value:

$$\varepsilon_w = \nu(\overline{b_u'^2} + \overline{b_w'^2}). \quad (18)$$

Moreover, even in the case of non-surface-disturbance, the limiting behaviour of k is,

$$\begin{aligned} k &= \frac{1}{2} \left\{ (\overline{a_u'^2} + \overline{a_w'^2}) + 2(\overline{a_u' b_u'} + \overline{a_w' b_w'}) y \right. \\ &\quad \left. + [\overline{b_u'^2} + \overline{b_v'^2} + \overline{b_w'^2} + 2(\overline{a_u' c_u'} + \overline{a_w' c_w'})] y^2 \dots \right\} \quad (19) \end{aligned}$$

which is obviously very different from that near a wall. Consequently, the relation that is appropriate near a wall:

$$\varepsilon = 2\nu \left(\frac{\partial \sqrt{k}}{\partial y} \right)^2 \simeq 2\nu k / y^2, \quad (20)$$

cannot be applied and hence Eq.(16) cannot be suitable to the free surface turbulence. Since the above discussion on the limiting behaviour does not produce useful results, the present study simply returns to

$$\varepsilon_P = k_P^{1.5} / (\beta c_\ell y_P), \quad (21)$$

that is usually used in the standard wall-function approach though coefficient β is multiplied to the length scale for modifying it to the free surface turbulence.

Concentration field modelling

As for the concentration of a solute, with a constant surface concentration condition, the surface limiting variations of the concentration and its fluctuation are

$$\begin{aligned} c &= a_c + b_c y + c_c y^2 + \dots, \\ c' &= b'_c y + c'_c y^2 + \dots. \end{aligned} \quad (22)$$

When the turbulent concentration flux $-\rho \overline{v'c}$ is modelled as $-\rho \overline{v'c} = \mu_t \partial c / \partial y$, the limiting variations lead to

$$-\rho \{ \overline{b'_c a'_v y} + (\overline{b'_c b'_v} + \overline{c'_c a'_v}) y^2 + \dots \} = \mu_t (b_c + 2c_c y + \dots). \quad (23)$$

Thus, the turbulent diffusivity behaves as $\mu_t \propto O(y)$. (In the case of non-surface-disturbance, $\mu_t \propto O(y^2)$ due to $a'_v = 0$ as discussed by Hasegawa & Kasagi, 2007.)

In the context of the eddy viscosity models, the turbulent scalar diffusivity μ_t is modelled using a turbulent Schmidt number as $\mu_t = \mu_t / (\mu Sc_t)$, thus with Eq.(7) one can rewrite this as

$$\mu_t = \kappa^* \max\{0, (y^* - y_n^*)\} / Sc_t \quad (24)$$

In order to satisfy the limiting behaviour of μ_t near the surface, the limiting behaviour is required as $Sc_t \propto O(y^{-1})$. Thus, as shown in Fig.1(b), Sc_t can be modelled as

$$Sc_t = \begin{cases} Sc_t^\infty / (y^* / y_c^*) & (0 \leq y^* \leq y_c^*), \\ Sc_t^\infty & (y_c^* < y^*), \end{cases} \quad (25)$$

where Sc_t^∞ is a constant for the region away from the surface. This simple two segment variation profile of Sc_t leads to the turbulent diffusivity distribution as in Fig.1(c):

$$\mu_t = \begin{cases} \alpha_c y^{*2} / Sc_t^\infty & (0 \leq y^* \leq y_c^*), \\ \kappa^* y^* / Sc_t^\infty & (y_c^* < y^*), \end{cases} \quad (26)$$

for the case of non-surface-disturbance where $\mu_t \propto O(y^2)$. The coefficient α_c and y_c^* have the relation: $\alpha_c = \kappa^* / y_c^*$ for connecting the two segments.

Note that, in the case of surface-disturbance and a constant surface flux condition, where $\mu_t \propto O(y^0)$, y_c should be 0.

Then, with the assumption that the right hand side terms can be constant over the cell, the simplified concentration equation in the surface adjacent cell P :

$$\frac{\partial}{\partial y^*} \left[\left(\frac{\mu}{Sc} + \mu_t \right) \frac{\partial c}{\partial y^*} \right] = \underbrace{\frac{\nu^2}{k_P} \left[\frac{\partial}{\partial x} (\rho u c) \right]}_{C_C}, \quad (27)$$

can be easily integrated analytically to form the boundary conditions of the concentration at the surface, namely the surface concentration flux:

$$q_s = - \frac{\mu}{Sc} \frac{d\overline{c}}{dy} \Big|_s = - \frac{k^{1/2}}{\nu} A_C, \quad (28)$$

or the mean surface concentration:

$$\overline{c}_s = \overline{c}_n + \frac{q_s Sc D_C}{\rho k_P^{1/2}} + \frac{Sc C_C E_C}{\mu}, \quad (29)$$

where the integration constants A_C , D_C and E_C are

$$A_C = \{ \mu (\overline{c}_n - \overline{c}_s) / Sc + C_C E_C \} / D_C, \quad (30)$$

$$D_C = \frac{1}{\alpha_{cd}^{1/2}} \tan^{-1} (\alpha_{cd}^{1/2} y_c^*) - \frac{1}{\alpha_{ct}} \ln \left(\frac{1 + \alpha_{ct} y_c^*}{1 + \alpha_{ct} y_n^*} \right), \quad (31)$$

$$\begin{aligned} E_C &= \frac{1}{\alpha_{ct}} (y_c^* - y_n^*) - \frac{1}{\alpha_{ct}^2} \ln \left(\frac{1 + \alpha_{ct} y_c^*}{1 + \alpha_{ct} y_n^*} \right) \\ &\quad - \frac{1}{2\alpha_{cd}} \ln (1 + \alpha_{ct} y_c^*), \end{aligned} \quad (32)$$

Table 2: Boundary conditions for the sheared free-surface flow.

	U	V	k	ε	\bar{c}
free surface	Eq.(13)	0	$\partial k/\partial y = 0$	Eq.(21)	Eq.(29)
free slip	$\partial U/\partial y = 0$	0	$\partial k/\partial y = 0$	$\partial \varepsilon/\partial y = 0$	$q_s = const.$

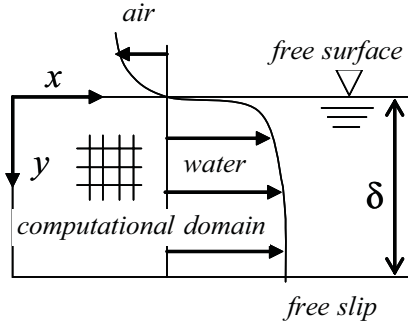


Figure 2: Computational domain of free surface flows.

with $\alpha_{ct} = \kappa^* Sc / Sc_t$ and $\alpha_{cd} = \alpha_{ct} / y_c^*$.

The presently optimized model coefficients for non-disturbance free-surface are listed in Table 1.

APPLICATION RESULTS

Computational conditions

The test case is a fully developed counter-current air-water flow driven by a constant pressure gradient studied by Hasegawa & Kasagi (2007) with the friction Reynolds number $Re_\tau = 150$. Fig.2 illustrates the coordinate system and the computational domain applied in the present computations. Only the water phase is solved with the non-disturbance and the constant concentration conditions at the free surface. At the bottom of the domain (lower boundary), a free slip and a constant concentration- flux conditions are imposed. The mean concentration field is solved by the eddy diffusivity model with a constant turbulent Schmidt number of 0.9. Table 2 summarises the presently applied boundary conditions of the turbulent quantities. Note that the AWF is not applied at the free slip boundary.

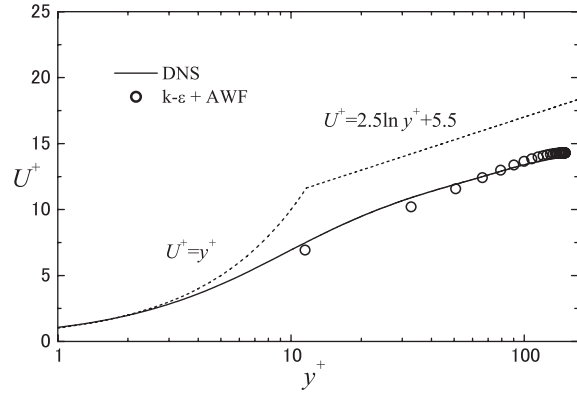
Since a constant concentration- flux condition is applied at the free slip boundary, a relatively fine grid resolution is used near there whilst the cell height facing to the interface is about $y^+ = 30$. Thus, computational grid used has $10(x) \times 25(y)$ cells non-uniformly distributed in the depth (y) direction.

Since the turbulent diffusivity near the free slip boundary behaves as $\kappa_t \propto O(y)$, it is necessary to damp it near the free slip boundary to obtain reasonable profiles of the concentration. Thus, in the present study, the following *ad hoc* form is employed:

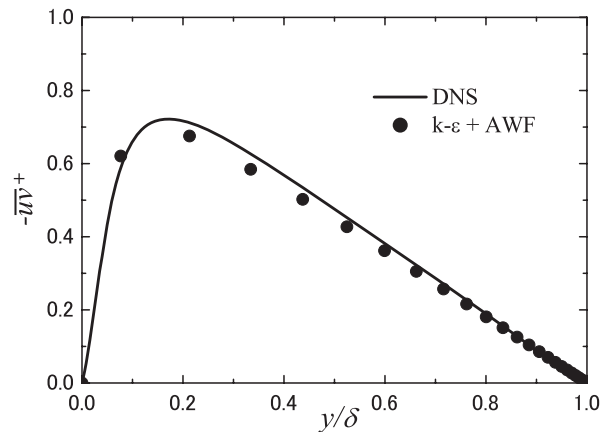
$$\kappa_t = \frac{\mu_t}{Sc_t} \times \min\{1, 2(1 - y/\delta)\}. \quad (33)$$

Results and discussions

Firstly, the standard $k - \varepsilon$ model is applied to the core flow region. The obtained flow field results are compared with the DNS data of Hasegawa and Kasagi (2007) in Figs.3(a) and (b). Fig.3(a) shows that the agreement between the present and the DNS results of the mean velocity



(a)



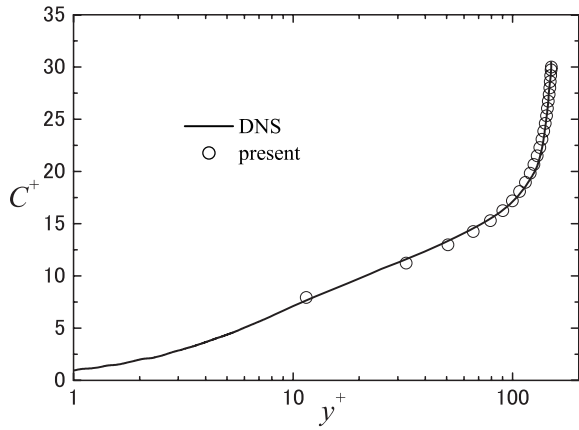
(b)

Figure 3: Flow field profiles: (a)mean velocity distribution, (b)Reynolds shear stress distribution.

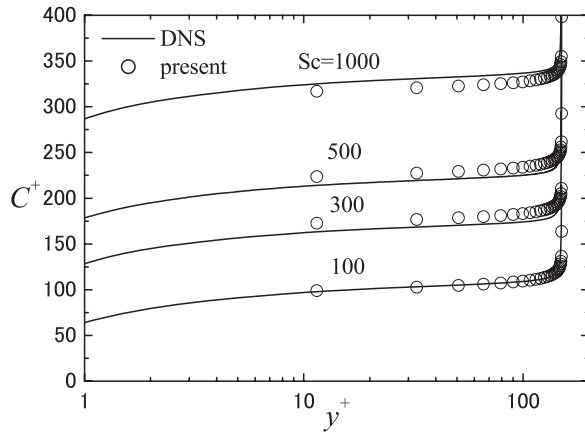
distribution is satisfactory and the profiles are significantly lower than that of the universal log line of wall turbulence. Fig.3(b) also confirms that the prediction ability of the present model for the Reynolds shear stress is satisfactory.

Figs.4(a) and (b) compare the mean concentration ($C^+ = |\bar{c} - \bar{c}_s| \rho u_\tau / q_s$) fields of $1 \leq Sc \leq 10^3$. All the present concentration profiles reasonably agree with the DNS results even at the high Schmidt numbers. This means that with the correct limiting variation of the turbulent diffusivity, the concentration fields can be reasonably captured by the AWF no matter how Sc is high.

For further evaluation of the model performance, the second moment closure of Craft & Launder (2001), which is called the TCL model, is also applied to the core region of the flow field. As for the boundary conditions of the Reynolds stresses, although each component has its own specific con-



(a)



(b)

Figure 4: Mean concentration distribution: (a) $Sc=1$, (b) $Sc=100-1000$.

dition at the free surface, simply the conditions:

$$\left. \frac{\partial(\overline{u_i u_i}/k)}{\partial y} \right|_P = 0, \quad (34)$$

and

$$-\rho \overline{uv}|_P = \mu_t \left. \frac{\partial U}{\partial y} \right|_P, \quad (35)$$

are imposed at node P. Fig.5 compares the mean velocity distribution and confirms that the present AWF also performs well with the second moment closure. However, as shown in Fig.6, the Reynolds normal stresses are not reproduced well particularly near the free surface. This is because the anisotropic distribution originates at the surface though the present AWF cannot determine the anisotropic distribution at the boundary.

CONCLUSIONS

For the case of non-surface-disturbance, the analytical wall function of free surface turbulence is proposed by modifying the version developed for wall turbulence. The scalar model for high Schmidt number concentration fields is also developed by considering the correct near-surface limiting behaviour of the turbulence quantities. The concluding remarks of the present study are:

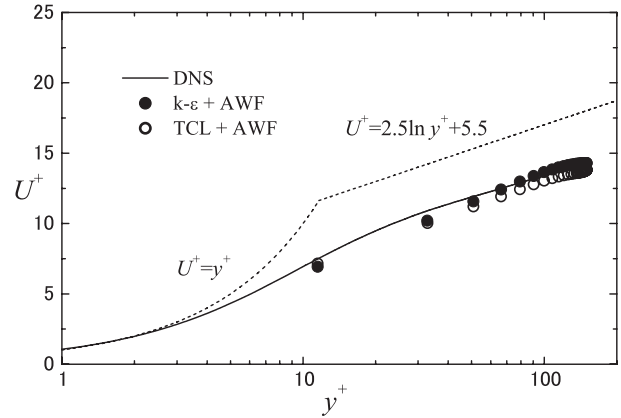


Figure 5: Comparison of the mean velocity distribution.

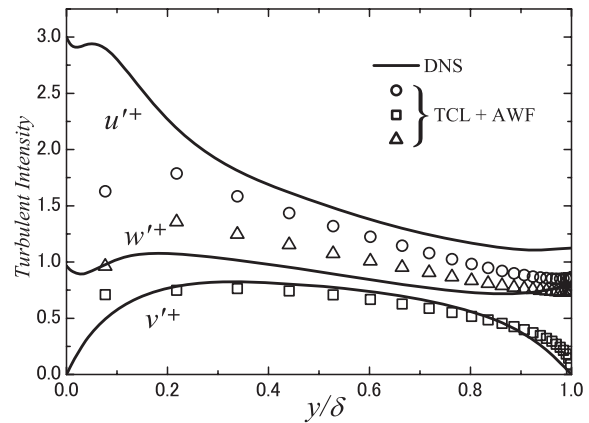


Figure 6: Reynolds normal stress distribution.

(1) By linking to the correct near-surface variation of the turbulent viscosity, the improved scheme has proven its good performance in a fully developed turbulent free surface flow with counter shear.

(2) For the scalar fields, the presently proposed scheme successfully reproduces the concentration fields at $1 \leq Sc \leq 1000$ by introducing the modelled turbulent diffusivity profile that satisfies the near-surface limiting behaviour.

(3) The proposed scheme is also applicable to a second moment closure. However, since the wall-function does not provide anisotropic distribution near the surface, the profiles of the Reynolds normal stresses near the surface are not satisfactory.

ACKNOWLEDGEMENTS

The authors thank Professors B.E. Launder, H. Iacovides and Dr. T.J. Craft of the University of Manchester for their fruitful collaboration at the initial stage of the present series of development of the AWF. A part of this work was financially supported by the Japan Society for the Promotion of Science through a Grant-in-Aid for Scientific Research (B) (No. 18360050).

REFERENCES

- Calmet, I., Magnaudet, J., 1998, "High-Schmidt number mass transfer through turbulent gas-liquid interfaces", *Int. J. Heat Fluid Flow*, Vol.19, pp.522–532.
- Craft, T.J., Gerasimov, A.V., Iacovides, H., Launder, B.E., 2002, "Progress in the generalization of wall-function treatments", *Int. J. Heat Fluid Flow*, Vol.23, pp.148–160.
- Craft, T.J., Launder, B.E., 2001, "Principles and performance of TCL-based second-moment closures", *Flow, Turb. Combust.*, Vol.66, pp.355–372.
- Hasegawa, Y., Kasagi, N., 2007, "Effects of interfacial velocity boundary condition on turbulent mass transfer at high Schmidt numbers", *Int. J. Heat Fluid Flow*, Vol. 28, pp.1192–1203.
- Herlina, Jirka, G.H., 2008, "Experiments on gas transfer at the air-water interface induced by oscillating grid turbulence", *J. Fluid Mech.*, Vol. 594, pp.183–208.
- Komori, S., Murakami, Y., Ueda, H., 1989, "The relationship between surface-renewal and bursting motions in an open-channel flow", *J. Fluid Mech.*, Vol. 203, pp.103–123.
- Komori, S., Nagaosa, R., Murakami, Y., Chiba, S., Ishii, K., Kuwahara, K., 1993, "Direct numerical simulation of three-dimensional open-channel flow with zero-shear gas-liquid interface", *Phys. Fluids A*, Vol.5, pp.115–125.
- Lombardi, P., De Angelis, V., Banerjee, S., 1996, "Direct numerical simulation of near-interface turbulence in coupled gas-liquid flow", *Phys. Fluids A*, Vol.6, pp.1643–1665.
- Rashidi, M., Banerjee, S., 1988, "Turbulence structure in free-surface channel flows", *Phys. Fluids*, Vol.31, pp.2491–2503.
- Suga, K., 2007, "Computation of high Prandtl number turbulent thermal fields by the analytical wall-function", *Int. J. Heat Mass Transfer*, Vol.50, pp.4967–4974.
- Suga, K., Abe, K., 2000, "Nonlinear eddy viscosity modelling for turbulence and heat transfer near wall and shear-free boundaries", *Int. J. Heat Fluid Flow*, Vol.21, pp.37–48.
- Suga, K., Craft, T.J., Iacovides, H., 2006, "An analytical wall-function for turbulent flows and heat transfer over rough walls", *Int. J. Heat Fluid Flow*, Vol.27, pp.852–866.
- Walker, J.W., Peirson, W.L., 2008, "Measurement of gas transfer across wind-forced wavy air-water interfaces using laser-induced fluorescence", *Exp. Fluids*, Vol.44, pp.249–259.